ELSEVIER

Journal of Alloys and Compounds 253–254 (1997) 241–247

Journal of ALLOYS AND COMPOUNDS

Neutron scattering studies of the structure and dynamics of rare-earth hydrides and deuterides

T.J. Udovic[a,*], J.J. Rush[a], Q. Huang[a,b], I.S. Anderson[c]

[a]*Materials Science and Engineering Laboratory, National Institute of Standards and Technology, Gaithersburg, MD 20899, USA*
[b]*Department of Materials and Nuclear Engineering, University of Maryland, College Park, MD 20742, USA*
[c]*Institut Laue-Langevin, 38042 Grenoble Cedex, France*

Abstract

The optic-vibrational density of states and the structural arrangement of hydrogen and/or deuterium dissolved in or compounded with the rare-earth metals ($RH(D)_x$ where $0<x\leq3$) have been measured by neutron vibrational spectroscopy (NVS) and neutron powder diffraction (NPD) for both the yttrium– and lanthanum–hydrogen systems. The spectra reflect the diversity in the phases encountered, from the α-phase solid solutions at low hydrogen concentrations to the superstoichiometric β-phase dihydrides above $x=2$ as well as the γ-phase trihydrides. The structure and dynamics of these systems are examined in detail for YH_x ($0<x\leq3$), where all three phases occur within the full concentration range, and LaH_x ($2\leq x\leq3$), where the fcc metal lattice remains the stable configuration up to the trihydride stoichiometry. In particular for LaH_x, NVS measurements of both pure and isotopically diluted samples indicate that the vibrational dynamics of hydrogen located in the octahedral (*o*) and tetrahedral (*t*) interstices are dramatically altered by the presence of significant *x*-dependent H–H interactions. NPD measurements are used for mapping out the *x*-dependent lattice symmetry due to the occurrence of long-range ordering of hydrogen in the *o* sublattice and as an aid in the interpretation of the vibrational spectra. In La hydrides prepared with H/D mixtures, both NVS and NPD confirm an isotopic enrichment of hydrogen in the *o* sublattice at low temperature.

Keywords: Hydrogen; Deuterium; Yttrium; Lanthanum; Neutron scattering

1. Introduction

The interaction of hydrogen with the rare-earth metals has been the subject of numerous investigations due to the interesting temperature- and concentration-dependent structures and properties observed in the α-phase solid solutions as well as the various ordered hydride phases [1]. Neutron scattering methods have been crucial for gaining a better understanding of the hydrogen binding potentials and ordering in these systems. In this paper, we present some previous as well as recent neutron scattering results from studies of two representative rare-earth/hydrogen(deuterium) systems: YH_x ($0<x\leq3$), where three different phases occur within the full concentration range, from an α-phase solid solution at low hydrogen concentrations, to the cubic dihydride β-phase for $2\leq x\leq2.10$, to the hcp trihydride γ-phase near $x=3$; and the light-rare-earth hydrides LaH_x ($2\leq x\leq3$), where the fcc metal lattice remains the stable configuration all the way up to the trihydride stoichiometry.

2. Experimental

Samples were typically synthesized by gas-phase absorption as discussed elsewhere [2,3]. To minimize the problems associated with sample impurities, only high-purity (99.99 at.%) metals and research grade H_2 and D_2 gases were used. For superstoichiometric β-phase samples in particular, the pure baseline dihydride or dideuteride was always formed by first evacuating any excess H or D above $x=2$ at 773 K, followed by adjustments in the stoichiometry by additional hydrogen or deuterium. Samples containing both hydrogen isotopes were synthesized using gas mixtures in the appropriate isotopic ratio.

The neutron scattering experiments were performed at the neutron beam split-core reactor (NBSR) at the National Institute of Standards and Technology. Neutron-vibrational-spectroscopy (NVS) measurements were made using the

*Corresponding author.

0925-8388/97/$17.00
PII S0925-8388(96)02885-X

BT-4 spectrometer with the Cu(220) monochromator and either the low-resolution Be or high-resolution Be-graphite–Be filter analyzer (with assumed final energies of 3 and 1.2 meV, respectively). Horizontal collimations before and after the monochromator ranged from 40' to 20' of arc depending on the desired instrumental resolution. The energy-dependent resolution (full width at half maximum) associated with a particular spectrum is denoted by horizontal bars beneath the peaks. Unless otherwise indicated, relative spectral scale factors in the figures are chosen so as to aid in lineshape comparisons, and spectral lines are drawn only as guides to the eye. Neutron-powder-diffraction (NPD) measurements were made using the BT-1, 32-detector, high-resolution, powder diffractometer with the Cu(311) monochromator at a wavelength of 1.5391(1) Å and horizontal divergences of 15', 20' and 7' of arc for the in-pile, monochromatic-beam and diffracted-beam collimators, respectively.

3. Yttrium–hydrogen

The neutron vibrational spectra of the different phases of YH_x are depicted in Fig. 1, illustrating marked differences in the H density of states (DOS). At low H concentrations below $x \approx 0.2$ [4], an α-phase solid solution exists with H residing in the tetrahedral (t) interstices of the hexagonal-close-packed (hcp) Y metal lattice and is stable down to near absolute zero. The α-$YH_{0.18}$ spectrum indicates an anisotropic t-site potential, with the high-energy peak at 134.2 meV due to the doubly-degenerate basal-plane vibrations and the soft mode at 100.1 meV due to the singlet vibration along the c direction. Electrical-resistivity [5], diffuse-elastic-neutron-scattering [6] and NVS [7] studies of this and similar rare-earth α-phase systems indicated a short-range ordering of pairs of H atoms (in second-nearest-neighbor t sites separated by a metal atom) into zigzag-shaped, c-axis-directed chains below 150–170 K. This ordering phenomenon is manifested by the high-resolution, 8-K DOS spectra of the H c-axis vibrations in α-$YH_{0.18}$ and α-$Y(H_{0.1}D_{0.9})_{0.19}$ [8] in Fig. 2. For α-$YH_{0.18}$, the c-axis vibrational peak is split, whereas a collapse of this splitting is observed for H in α-$Y(H_{0.1}D_{0.9})_{0.19}$. This is evidence that the splitting in α-$YH_{0.18}$ is due to dynamic coupling between paired hydrogens with the split features associated with local acoustic (in-phase) and optic (out-of-phase) mode vibrations of the H in these pairs. In α-$Y(H_{0.1}D_{0.9})_{0.19}$, the H atoms are diluted by the heavier D atoms, minimizing the formation of H–H pairs necessary for dynamic coupling to occur. Such isotope-dilution-neutron-spectroscopy studies have been utilized extensively in what follows to examine the details of dynamic interactions and related structural properties of rare-earth-hydride systems. From one-dimensional modelling of the 4-meV splitting associated with the α-$YH_{0.18}$ c-axis feature, the H–H interaction force constant was estimated to be ~4% of the Y–H force constant [8].

Above $x \approx 0.2$, YH_x precipitates out into the β-phase dihydride β-YH_2, forming a face-centered-cubic (fcc) Y lattice with H fully occupying the t interstices. For $2 < x \leq 2.10$, the excess H atoms partially occupy the octahedral (o) interstices. This can be seen clearly by the H DOS spectra for β-YH_2 [9] and β-$YH_{2.10}$ in Fig. 1. The pure dihydride spectrum yields a broad complex doublet centered at ~123 meV due to the vibrations of the t-site H (H_t) atoms. The superstoichiometric dihydride β-$YH_{2.10}$ possesses a similar feature as well as a small lower-energy

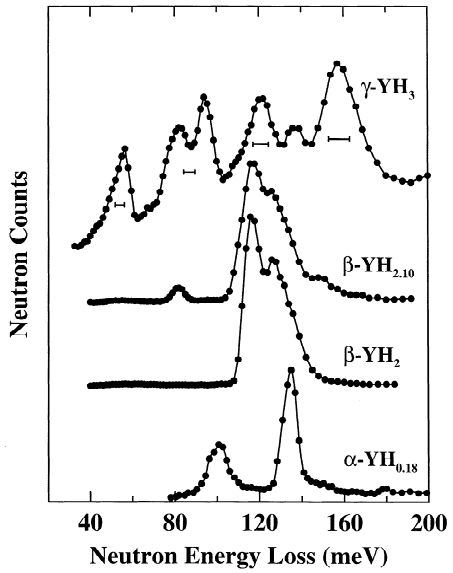

Fig. 1. Comparison of the low-resolution vibrational spectra for α-$YH_{0.18}$, β-YH_2 [9], β-$YH_{2.10}$ and γ-YH_3 at low temperature.

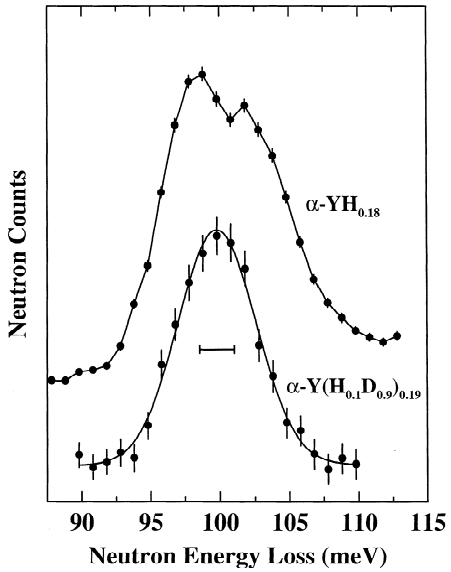

Fig. 2. High-resolution H vibrational spectra of the c-axis-polarized modes in α-$YH_{0.18}$ and α-$Y(H_{0.1}D_{0.9})_{0.19}$ at 8 K [8].

feature at 81.2 meV due to the vibrations of the *o*-site H (H_o) atoms. The lack of H_o vibrations in the β-YH_2 spectrum is somewhat contrary to the belief [10] that *o* sites begin filling in the pure rare-earth dihydrides before the full occupation of the *t* sites. Indeed, recent NPD measurements of β-YD_2 [11] also infer full *t*-site occupation and zero *o*-site occupation within statistical uncertainty, at least up to ~600 K. This is in agreement with recent magic-angle-spinning NMR results for β-YD_x at 200 K [12], which indicated only *t*-site occupation for $x<2.00$.

Isotope-dilution experiments have shown that the complex vibrational DOS for the H_t atoms is a manifestation of H–H dynamic interactions, similar to that observed for the H–H pairing interactions in α-YH_x. Such interactions were invoked years ago to describe the origin of a similar optic-phonon dispersion for the H_t vibrations in the cubic dihydride ZrH_2 [13]. In particular, diluting the H atoms with heavier D atoms in the β-phase dihydride has been seen to cause a collapse of the dynamically induced dispersion into a much sharper singlet feature representative of the triply-degenerate normal modes of an isotopically-isolated H_t atom situated in a cubic potential [9]. Fig. 3 illustrates this for the reverse case of isotope dilution, i.e., D atoms diluted by lighter H atoms in β-$Y(H_{0.9}D_{0.1})_2$ [9]. The relative collapse of the split D_t DOS into a narrow peak in going from β-YD_2 to β-$Y(H_{0.9}D_{0.1})_2$ clearly reflects the result of isolating the D_t atoms from each other. Moreover, the weak sidebands in the diluted D_t DOS can be attributed to local acoustic- and optic-mode vibrations from a smaller number of isolated nearest-neighbor D_t–D_t pairs. From the 5-meV splitting in this case, the nearest-neighbor D_t–D_t interaction force constant can be estimated to be ~6% of the Y–D force constant.

Near the upper β-phase boundary, there are indications [14,15] that the H_o atoms develop a short-range-ordered arrangement akin to the long-range ($I4/mmm$) order expected for the hypothetical cubic $YH_{2.25}$ stoichiometry, in which only every fourth (042) *o*-site plane is occupied by hydrogen. This behavior is consistent with the low-temperature vibrational spectra of the H_o atoms in β-$YH_{2.03}$ and β-$YH_{2.10}$ in Fig. 4. The H_o spectra display a similar concentration dependence as those for the superstoichiometric dihydrides of Tb [16] and La [17]. In all these systems, the H_o DOS is found to be sensitive to the temperature- and concentration-dependent arrangement of the H_o atoms in the *o*-site sublattice. For $x=2.03$, the low-concentration H_o atoms are predominantly isolated in a local cubic environment and possess a sharp DOS. Minor sideband contributions are attributed to the small fraction of H_o atoms that participate in small clusters of short-range order at this H_o concentration. As *x* increases to 2.10, the extent of the short-range order increases, as evidenced by the growth of the sidebands with respect to the central feature. If there were no β/γ phase boundary at this H_o concentration (such as for β-TbH_x and β-LaH_x), then the order for $x>2.10$ would most likely become long-ranged. In this case, approaching $x=0.25$ would lead to full $I4/mmm$ order with the disappearance of the central feature and the growth of the sidebands into a dispersion-broadened bimodal DOS distribution (e.g., see the $LaH_{2.25}$ spectrum in Fig. 7 below and the accompanying mode assignments in the text).

In actuality, for H concentrations above $x=2.10$, γ-phase YH_3 precipitates out, reverting back to an hcp metal lattice, which is typical of the other heavier rare-earth

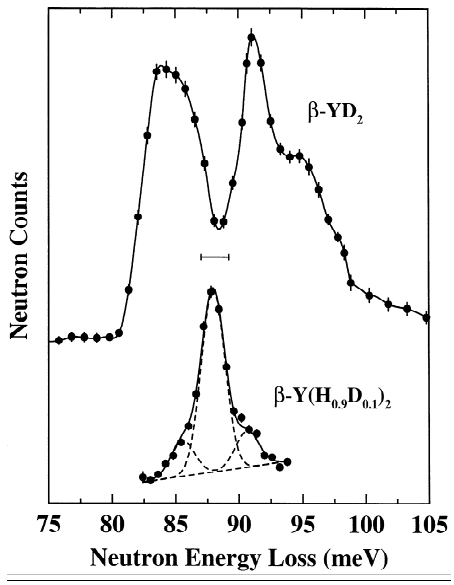

Fig. 3. High-resolution D_t vibrational spectra for β-YD_2 and β-$Y(H_{0.9}D_{0.1})_2$ at low temperature. A multicomponent Gaussian fit of the latter shows a strong central peak associated with the vibrations of isolated D_t atoms and a weaker doublet assigned to the acoustic and optic vibrations of D_t–D_t pairs [9].

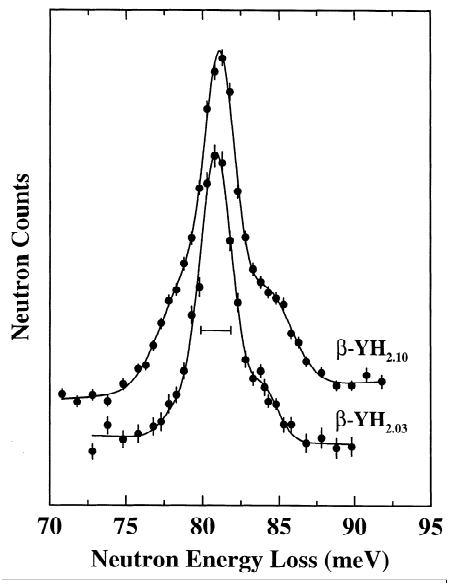

Fig. 4. High-resolution H_o vibrational spectra for β-$YH_{2.03}$ and β-$YH_{2.10}$ at 10 K.

trihydride systems [18,19]. Recent NPD results for YD_3 [3] are in agreement with an earlier study [20] and indicate a structure possessing $P\bar{3}c1$ symmetry, identical to that found for HoD_3 [21]. In this structure, the unit cell is a $(\sqrt{3}\times\sqrt{3})R30°$ expansion of the conventional hcp unit cell in the *ab* plane (i.e., $a=\sqrt{3}a_0$, $c=c_0$). The D atoms occupy unusual interstitial positions of a *c*-axis-elongated hcp metal lattice, instead of the more conventional *o* and *t* sites. The D_o atoms are displaced vertically toward the metal planes from their ideal *o*-site positions, with one-third and two-thirds of the atoms located at in-plane (*m*1) and near-plane (*m*2) three-fold positions, respectively (see Fig. 5). The D_t atoms are displaced horizontally also in a correlated fashion to accommodate the presence of the *m*-site D (D_m) atoms. Moreover, the NPD refinements suggest the presence of an order-disorder equilibrium amongst the D_m atoms. The disorder involves *c*-axis displacements of a fraction of D_m atoms from near-plane to in-plane positions, concomitant with an equal number of compensating D_m atoms shifting from in-plane to near-plane positions. The displacements are facilitated by the relatively open channels formed along the *c* direction by the Y and D_t atoms. The γ-YH_3 spectrum in Fig. 1 shows the complexity of the H vibrational DOS. A complete mode assignment of the spectrum is in progress. Considering the sizes and geometries of the *m* and *t* sites, it is believed that the *c*-axis-polarized vibrations of the H_m atoms account for the lowest-energy asymmetric feature at 57 meV. A high-resolution spectrum of this feature is suggestive of a bimodal lineshape. Thus, based on relative occupancies, the in-plane H_m atoms are tentatively assigned to a weaker component at ~52 meV and the near-plane H_m atoms to a stronger component at ~57 meV. Indeed, one would expect the in-plane H_m atoms to have a lower normal-mode energy since the corresponding Y–H force constants have no vector component in the *c* direction (unlike the Y–H force constants associated with the near-plane H_m atoms).

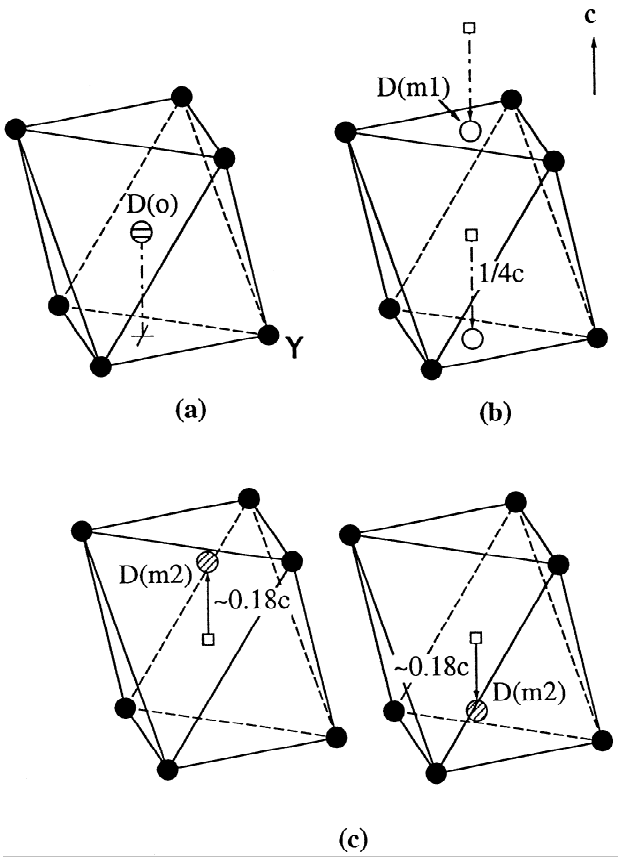

Fig. 5. The displacement of the D atoms from (a) the hypothetical ideal *o* sites defined by the hcp metal sublattice to (b) the in-metal-plane and (c) the near-metal-plane *m* sites in the actual γ-YD_3 structure.

4. Lanthanum–hydrogen

Unlike YH_x, the light rare-earth hydride LaH_x maintains its fcc metal sublattice over the entire concentration range $2\leq x\leq 3$. This leads to a more complicated phase diagram [22] and more significant and variegated H–H interactions over the large H-concentration range. This is mirrored by the low-temperature H vibrational spectra for the *x*-dependent series of La hydrides in Fig. 6. Upon increasing the H concentration from $x=2$ (where the spectrum reflects only H_t vibrations) to $x=3$, the H_t DOS (i.e., the features above ~80 meV) transforms into a complex distribution of peaks due to *x*-dependent H_t–H_o and H_t–H_t interactions [2]. Concomitantly, the contributions from the H_o DOS emerge and grow in a way dictated by *x*-dependent H_o–H_o interactions. In particular, as discussed earlier for the β-YH_x spectra in Fig. 4, the relatively sharp DOS at 70.7

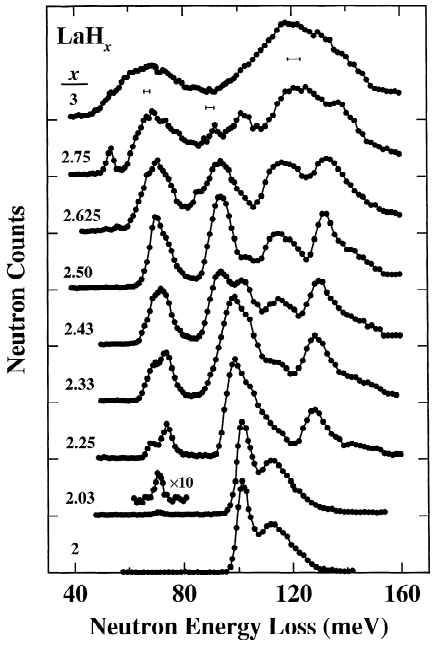

Fig. 6. High-resolution vibrational spectra for LaH_x ($2\leq x\leq 3$) near 10 K.

meV for the predominantly isolated H_o atoms in $LaH_{2.03}$ transforms into a broadened bimodal distribution at 68.3 and 74.0 for $LaH_{2.25}$ [17]. The latter H_o DOS is a reflection of the $I4/mmm$ order which is stabilized at low temperature. Fig. 7 illustrates the ideal low-temperature $LaD_{2.25}$ structure as determined by NPD [23], an arrangement typically observed for other rare-earth deuterides near this stoichiometry [24–26]. The long-range order in the H_o sublattice of $LaH_{2.25}$ is accompanied by a cubic-to-tetragonal lattice distortion. In this structure, all nearest-neighbor *o* sites surrounding the H_o atoms are vacant, an observation which has prompted others [25] to suggest that a repulsive H_o–H_o interaction drives the H_o ordering in these systems. Due to the presence of significant *x*-dependent H–H interactions in these systems, the local site symmetry of the H_o atoms may no longer be considered to be cubic, since the positions of the surrounding H_o neighbors must also be included. Consideration of the noncubic symmetry of the $I4/mmm$-ordered H_o sublattice in $LaH_{2.25}$ and the relative intensities of the bimodal peaks

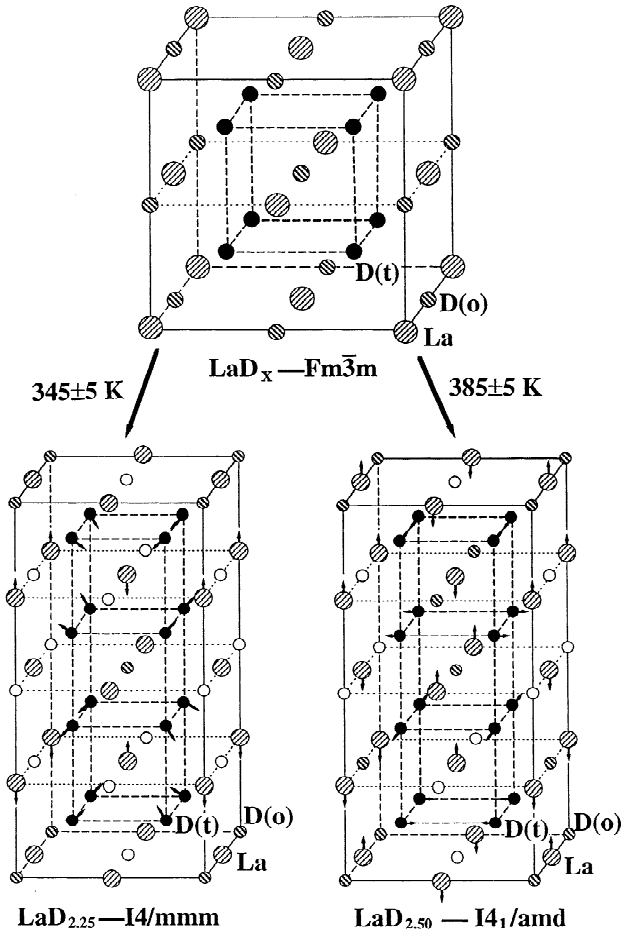

Fig. 7. Comparison of the low-temperature structures for $LaD_{2.25}$ ($I4/mmm$) [23] and $LaD_{2.50}$ ($I4_1/amd$) [27] as determined by NPD. Arrows indicate the displacement directions of the D_t and La atoms from the high-symmetry positions. In the high-temperature cubic structures, the partially filled D_o sublattices are completely disordered.

leads to the assignment of the stronger, higher-energy component to degenerate H_o vibrational modes polarized in the *ab* plane and the weaker, lower-energy component to the orthogonal singlet H_o vibrational mode polarized along the *c* direction. This suggests similar assignments for the spectral sidebands found for the H_o DOS in β-$YH_{2.10}$ in Fig. 4 above, except in that case, the H_o ordering is shorter-ranged.

As the H concentration increases to $LaH_{2.50}$, the relative intensities of the bimodal components of H_o DOS become reversed and further broadened. In this instance, the ideal, low-temperature, long-range-ordered structure as determined for $LaD_{2.50}$ by NPD [27] has $I4_1/amd$ symmetry (see Fig. 7), similar to that observed for $CeD_{2.45}$ [28]. The H_o ordering can be described as a repeating sequence of four (042) *o*-site planes comprised of two adjacent filled planes followed by two adjacent empty planes. Again, based on symmetry and relative intensity arguments, the stronger, lower-energy component of the H_o DOS would be assigned to the degenerate H_o vibrational modes polarized in the *ab* plane and the weaker, higher-energy component to the orthogonal H_o vibrational mode polarized along the *c* direction. This is in contrast to the assignment in $LaH_{2.25}$, where the *c*-axis mode is the softer mode, yet is qualitatively consistent with the differences in the two structures. In particular, the inclusion of the extra H_o atoms into the $LaH_{2.25}$ structure to make the $LaH_{2.50}$ structure leads to the occupation of four out of the twelve nearest-neighbor *o*-site vacancies surrounding each H_o atom. This results in additional H_o–H_o force constant contributions to the *o*-site potentials. Because of the $LaH_{2.50}$ symmetry, all four nearest-neighbor H_o atoms perturb the *c*-axis vibrations, whereas only two of the four nearest-neighbor H_o atoms perturb each of the degenerate orthogonal vibrations in the *ab* plane. Thus, ignoring all other effects which appear to cause the mean H_o vibrational energy to decrease with increasing H_o concentration, we would suggest that the extra H_o atoms in $LaH_{2.50}$ cause the *c*-axis vibrations to stiffen more than the *ab*-plane vibrations, probably enough to place the *c*-axis-mode energy above the doubly-degenerate-mode energies.

Fig. 8 illustrates the effects of D–D interactions on the D_o DOS for $LaD_{2.50}$ by a comparison with the D_o DOS for $La(H_{0.9}D_{0.1})_{2.50}$. Similar to the isotope dilution results for α-$YH_{0.18}$ and β-YD_2 in Figs. 2 and 3 above, dilution of the D atoms with the lighter H atoms causes a collapse of the D_o DOS into a much sharper feature. Again, this is evidence for the presence of significant dynamic coupling interactions within the D_o sublattice of $LaD_{2.50}$ as the origin of the vibrational line broadening. A similar result was observed previously for the H_o DOS spectra for β-$TbH_{2.25}$ and β-$Tb(H_{0.1}D_{0.9})_{2.25}$ [2], which corroborates the generality of these β-phase interactions for different *x* values and for different rare-earth hydrides.

The H DOS for $LaH_{2.75}$ in Fig. 6 is worthy of mention due to the emergence of unusual features at 53.4, 92, and

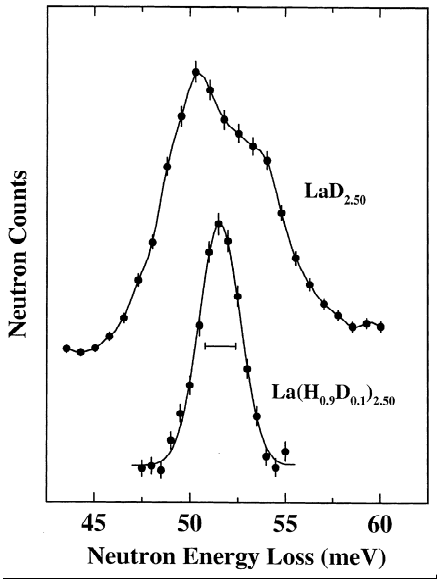

Fig. 8. Comparison of the high-resolution D_o vibrational spectra for $LaD_{2.50}$ and $La(H_{0.9}D_{0.1})_{2.50}$ at 10 K.

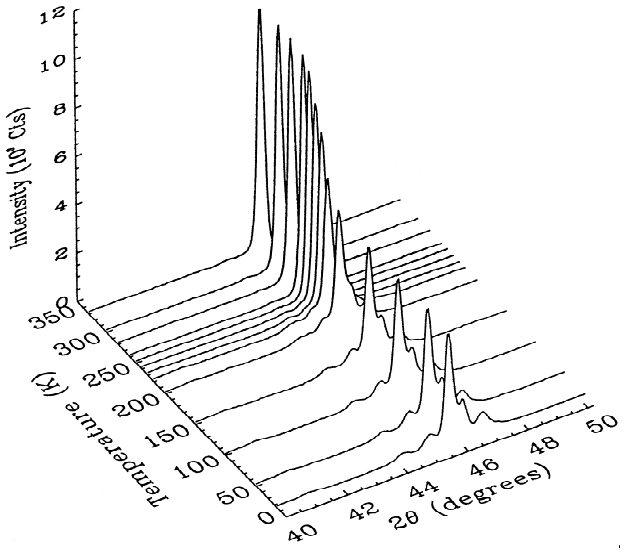

Fig. 9. Temperature dependence of the Bragg scattering around the [220] reflection for LaD_3.

102 meV. These features appear to smear out or disappear as the temperature is increased above the tetragonal-to-cubic phase transition near 240 K. Low-temperature NPD measurements of $LaD_{2.75}$ [29] are suggestive of the presence of a minor second phase of unknown structure besides a main tetragonal phase possessing long-range D_o ordering. Further experiments are underway to determine whether these DOS features may indeed be related to the presence of some low-temperature secondary phase.

At the highest H concentration, LaH_3, the two extremely broad H_o and H_t components of the H DOS in Fig. 6 reflect considerable optic-phonon dispersion due to the presence of extensive H–H interactions. Previous heat-capacity studies [30] suggested a complicated temperature-dependent evolution in structure. Early NPD measurements of LaD_3 [31] confirmed at least one phase transition at ~230 K as evidenced by the appearance of low-temperature superlattice peaks. This has been confirmed by more recent high-resolution NPD measurements of LaD_3 [32] which reveal the emergence with cooling, of additional satellite lines associated with the main Bragg features. For example, Fig. 9 illustrates the temperature dependence of the Bragg scattering around the [220] reflection. A transformation from the cubic structure occurs below ~260 K with a redistribution of some scattering intensity away from the main [220] peak and into a series of closely-spaced satellite lines. This is different behavior than has been typically observed during the transitions of La deuterides having lower D concentrations, and structural models are currently being considered to explain the results.

Finally, preliminary investigations have been undertaken in order to characterize more carefully the H and D site distributions in mixed-isotope rare-earth hydrides. In particular, both NPD and NVS measurements of $La(H_{1-y}D_y)_{2.50}$ $(0 \leq y \leq 1)$ confirm that an isotopic enrichment of H with respect to D occurs in the *o*-sites and is maximized at low temperature. For example, for $La(H_{0.2}D_{0.8})_{2.50}$, Rietveld refinements of diffraction data have indicated that the H/D isotopic ratio in the *o*-site sublattice varies from 41/59 at 15 K to 30/70 at 300 K and 26/74 at 400 K. The range of values is significantly different from the overall H/D stoichiometric ratio of 20/80. The physics behind this phenomenon is currently being explored in more detail.

5. Conclusions

The above neutron scattering results for the Y and La hydrides and deuterides are representative of the interesting physics which occurs for all the rare-earth hydrides due to the *x*-dependent interactions of the hydrogen isotopes in the complex array of phases present. Clearly, more work needs to be done to fully characterize the hydrogen binding potentials and their effect on the structural and dynamic behavior in these systems. These results indicate that further progress can be made in this area using the unique capabilities of neutron scattering methods in combination with isotopically manipulated hydride samples.

References

[1] P. Vajda, in K.A. Gschneidner and L. Eyring (eds.), *Handbook on the Physics and Chemistry of Rare Earths*, Vol. 20 Elsevier Science, 1995, p. 207, and references therein.

[2] T.J. Udovic, J.J. Rush and I.S. Anderson, *J. Alloys Comp.*, 231 (1995) 138.

[3] T.J. Udovic, Q. Huang and J.J. Rush, *J. Phys. Chem. Solids*, 57 (1996) 423.
[4] P. Vajda, J.N. Daou, A. Lucasson and J.P. Burger, *J. Phys. F*, 17 (1987) 1029.
[5] J.N. Daou and P. Vajda, *Ann. Chim. Fr.*, 13 (1988) 567.
[6] O. Blaschko, *J. Less-Common Met.*, 172–174 (1991) 237, and references therein.
[7] T.J. Udovic, J.J. Rush, N.F. Berk, I.S. Anderson, J.N. Daou, P. Vajda and O. Blaschko, *Z. Phys. Chem.*, 179 (1993) 349, and references therein.
[8] I.S. Anderson, N.F. Berk, J.J. Rush and T.J. Udovic, *Phys. Rev. B*, 37 (1988) 4358.
[9] T.J. Udovic, J.J. Rush and I.S. Anderson, *Phys. Rev. B*, 50 (1994) 15 739.
[10] J.A. Goldstone, J. Eckert, P.M. Richards and E.L. Venturini, *Solid State Commun.*, 49 (1984) 475.
[11] T.J. Udovic, Q. Huang, F. Altorfer and J.J. Rush, unpublished.
[12] N.L. Adolphi, J.J. Balbach, M.S. Conradi, J.T. Markert, R.M. Cotts and P. Vajda, *Phys. Rev. B*, 53 (1996) 15 054.
[13] E.L. Slaggie, *J. Phys. Chem. Solids*, 29 (1968) 923.
[14] J.N. Daou and P. Vajda, *Phys. Rev. B*, 45 (1992) 10 907.
[15] S.N. Sun, Y. Wang and M.Y. Chou, *Phys. Rev. B*, 49 (1994) 6481.
[16] T.J. Udovic, J.J. Rush and I.S. Anderson, *Phys. Rev. B*, 50 (1994) 7144.
[17] T.J. Udovic, J.J. Rush and I.S. Anderson, *J. Phys.: Condens. Matter*, 7 (1995) 7005.
[18] G.E. Sturdy and R.N.R. Mulford, *J. Am. Chem. Soc.*, 78 (1956) 1083.
[19] A. Pebler and W.E. Wallace, *J. Phys. Chem.*, 66 (1962) 148.
[20] N.F. Miron, V.I. Shcherbak, V.N. Bykov and V.A. Levdik, *Sov. Phys. Crystallog.*, 17 (1972) 342 [*Krystallografiya*, 17 (1972) 404].
[21] M. Mansmann and W.E. Wallace, *J. Phys. (Paris)*, 25 (1964) 454.
[22] K. Conder, L. Wang, E. Boroch and E. Kaldis, *Eur. J. Solid State Inorg. Chem.*, 28 (1991) 487.
[23] T.J. Udovic, Q. Huang, J.J. Rush, J. Schefer and I.S. Anderson, *Phys. Rev. B*, 51 (1995) 12 116.
[24] V.K. Fedotov, V.G. Fedotov, M.E. Kost and E.G. Ponyatovskii, *Sov. Phys. Solid State*, 24 (1982) 1252 [*Fiz. Tverd. Tela (Leningrad)*, 24 (1982) 2201].
[25] G. André, O. Blaschko, W. Schwarz, J.N. Daou and P. Vajda, *Phys. Rev. B*, 46 (1992) 8644.
[26] Q. Huang, T.J. Udovic, J.J. Rush, J. Schefer and I.S. Anderson, *J. Alloys Comp.*, 231 (1995) 95.
[27] T.J. Udovic, Q. Huang and J.J. Rush, *J. Solid State Chem.*, 122 (1996) 151.
[28] R.R. Arons, in H.P.J. Wijn (ed.), *Landolt-Börnstein, New Series III*, Vol. 19d1, Springer-Verlag, Berlin, 1991, p. 280.
[29] T.J. Udovic, Q. Huang, J.J. Rush, J. Schefer and I.S. Anderson, unpublished.
[30] T. Ito, B.J. Beaudry, K.A. Gschneidner, Jr. and T. Takeshita, *Phys. Rev. B*, 27 (1983) 2830.
[31] J.J. Didisheim, K. Yvon, P. Fischer, W. Hälg and L. Schlapbach, *Phys. Lett.*, 78A (1980) 111.
[32] T.J. Udovic, Q. Huang and J.J. Rush, unpublished.